대한조선학회논문집 Research Paper
Journal of the Society of Naval Architects of Korea
eISSN:2287-7355, Vol. 59, No. 6, pp. 338-344, December 2022
https://doi.org/10.3744/SNAK.2022.59.6.338

CFD 해석을 활용한 선박의 순수 횡동요 시험 연구

마이티로안[1] · 보안코아[1] · 윤현규[2,†]
창원대학교 스마트환경에너지공학과[1]
창원대학교 조선해양공학과[2]

Study on Pure Roll Test of a Ship Using CFD Simulation

Thi Loan Mai[1]·Anh Khoa Vo[1]·Hyeon Kyu Yoon[2,†]
Dept. of Smart Environmental Energy Engineering, Changwon National University[1]
Dept. of Naval Architecture and Marine Engineering, Changwon National University[2]

Roll moment usually is ignored when analyzing the maneuverability of surface ships. However, it is well known that the influence of roll moment on maneuverability is significant for ships with small metacentric height such as container ships, passenger ships, etc. In this study, a pure roll test is performed to determine the hydrodynamic derivatives with respect to roll motion as added mass and damping. The target ship is an autonomous surface ship designed to carry containers with a small drift and large freeboard. The commercial code of STAR CCM+ software is applied as a specialized tool in naval hydrodynamic based on RANS equation for simulating the pure roll of the ship. The numerical uncertainty analysis is conducted to verify the numerical accuracy. By distinguishing the in-phase and out-of-phase from hydrodynamic forces and moments due to roll motion, added mass derivatives and damping derivatives relative to roll angular velocity are obtained.

Keywords : Pure roll test, Autonomous surface ship, CFD simulation, Hydrodynamic derivatives

1. Introduction

Ship maneuverability is typically described based on 3-DOF (degrees of freedom) motion equations including surge, sway, and yaw, while roll motion has been ignored as a secondary one. However, the roll motion is significantly affected for ships with small metacentric heights such as container ships, passenger ships due to large heel motion, which makes a considerable effect on maneuvering motion.

Research on the maneuverability characteristics including the roll effect was already done in several studies. Son and Nomoto (1982) conducted the 4-DOF maneuvering simulation of an S-175 container ship. To capture the roll effect on the ship, they performed an Oblique Towing Test (OTT) with variations in the heel angle. The derivatives with respect to lateral velocity and heel angle were obtained. Yasukawa and Yoshimura (2014) presented the ship maneuverability for three kinds of ships as container ship, pure car carrier, and ferry considering roll considering roll-coupling effect. The roll-coupling derivatives were obtained from the OTT and Circular Motion Test (CMT) with different the roll angle to take the derivatives including yaw angular velocity relative derivatives. Fukui et al. (2016) introduced the 4-DOF mathematical model for maneuvering simulation. The effect of the roll angle on the hydrodynamic derivatives was found by carrying out the circular motion test with setting a constant roll angle. By performing the free running model test of container ship and passenger ferry at different metacentric height, they concluded that the small metacentric height and high ship speed lead to the course stability unstable side. Yasukawa et al. (2019) proposed the maneuvering simulation of 3-DOF motion equation conventionally considering the roll-coupling by adding the motion equation of the roll to become 4-DOF model. In which roll moment acting on the hull was obtained by multiplying the hull lateral force to the vertical acting point. The roll-related derivative and the vertical acting point of the lateral forces was estimated by simple formulas.

Received : 11 July 2022 | Revised : 13 September 2022 | Accepted : 8 October 2022
† Corresponding author : Hyeon Kyu Yoon, hkyoon@changwon.ac.kr

From the literature review just presented, mainly focused on the roll-coupling effect based on the static test of OTT and CMT at different roll angles. Therefore, the obtained derivatives were the coupling derivatives with respect to lateral velocity and roll angle, yaw angular velocity and roll angle. However, a component of added mass of roll was not mentioned in these studies due to difficulty performing using the experimental method. Unlike pure sway and pure yaw motions, the pure roll motion is required the complex devices. For example, Park et al. (2015) introduced the conning motion test equipment to execute the pure roll and 6-DOF combined test of submerged body. Besides, Kim et al. (2021) also developed the apparatus for the pure roll motion test for the underwater vehicle. Nonetheless, those methods are difficult for applying to the surface ship.

This study simulates the pure roll test of an autonomous surface ship designed to carry the containers based on the Computational Fluid Dynamics (CFD) method in STAR CCM+. The simulation method is verified by performing the mesh independent study with three grid densities of fine, medium, and coarse. Then, the forces and moments is calculated at various dimensionless roll angular velocity. The added mass and damping derivatives relative to roll components are obtained by distinguishing in-phase and out-of-phase from hydrodynamic forces and moments during pure roll test.

2. Numerical analysis

2.1 Coordinate system

Considering the vertical plane for the roll motion, two-right hand coordinate system including body-fixed coordinate system $o-y_bz_b$ and earth-fixed coordinate system $o-yz$ are employed to define the kinematic and hydrodynamic forces acting on the ship. Fig. 1 shows the coordinate system of roll motion with z-axis points vertically downwards and y-axis

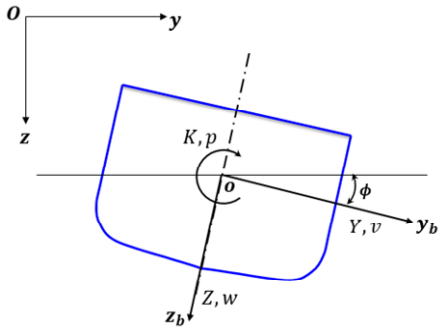

Fig. 1 Coordinate system of roll motion

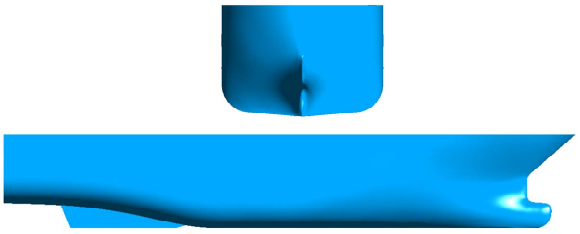

Fig. 2 Model geometry

Table 1 Main specification of the ship

Item	Symbol (unit)	Value
Length perpendicular	*Lpp* (m)	22.00
Breadth	*B* (m)	6.00
Draft	*T* (m)	1.25
Height to deck	*H* (m)	4.14
Volume	∇ (m^3)	85.68
Design speed	*U* (knots)	13

points to starboard. Roll angle is denoted by ϕ. v and w are the sway and heave velocity, respectively. p indicates the roll angular velocity.

2.2 Objective and test condition

The target ship used in this study is an autonomous surface ship designed to carry the containers with small draft and large freeboard. The ratio of design draft to ship's height is 1/3.3. This is one reason to increase the influence of roll moment. Fig. 2 displays the full-scale ship which is applied in numerical simulation. Table 1 lists the main particulars of the ship.

The pure roll is conducted for the full-scale ship at the design speed of 13 knots in STAR CCM+ program. The condition for the pure roll motion is given with various dimensionless roll angular velocities (p') by a range of 0.1 ~ 0.6. Due to changing of roll angle (ϕ_0), the frequency of the motion is calculated as equal to 3.125 rad/s based on the equation of $p=\frac{\phi_0\omega U}{L}$.

2.3 Pure roll

The pure roll of the ship is a harmonic angular motion by the x-axis at a constant speed. The condition that must be satisfied is the roll angle (ϕ) varies with time. It is

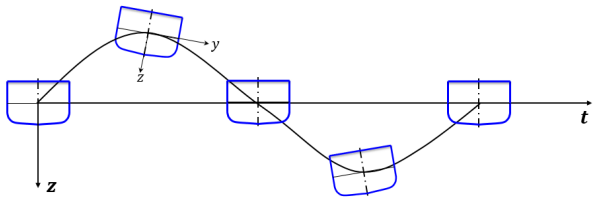

Fig. 3 Pure roll

performed with a given dimensionless angular velocity (p'). Fig. 3 presents the pure roll motion of the surface ship. Eq. (1) describes the function of pure roll with roll angle (ϕ), roll angular velocity (p'), and roll acceleration ($\dot{p}'$).

$$\phi = \phi_0 \sin(\omega t) \tag{1}$$

$$p = \dot{\phi} = \phi_0 \omega \cos(\omega t)$$

$$\dot{p} = \ddot{\phi} = -\phi_0 \omega^2 \sin(\omega t)$$

where, ϕ_0 is the amplitude of roll motion. The mathematical model of hydrodynamic force acting on the ship during the pure roll can be expressed as,

$$Y = Y_{\dot{p}}\dot{p} + Y_p p + Y_{ppp}p^3 \tag{2}$$

$$K = K_{\dot{p}}\dot{p} + K_p p + K_{ppp}p^3$$

$$N = N_{\dot{p}}\dot{p} + N_p p + N_{ppp}p^3$$

Substituting Eq. (1) into Eq. (2), the equation of the pure roll can be written as

$$Y = Y_{\dot{p}}\left(-\phi_0\omega^2 \sin\omega t\right) + Y_p(\phi_0 \omega \cos\omega t) + Y_{ppp}(\phi_0 \omega \cos\omega t)^3 \tag{3}$$

$$K = K_{\dot{p}}\left(-\phi_0\omega^2 \sin\omega t\right) + K_p(\phi_0 \omega \cos\omega t) + K_{ppp}(\phi_0 \omega \cos\omega t)^3$$

$$N = N_{\dot{p}}\left(-\phi_0\omega^2 \sin\omega t\right) + N_p(\phi_0 \omega \cos\omega t) + N_{ppp}(\phi_0 \omega \cos\omega t)^3$$

The hydrodynamic force during the pure roll can be decomposed into in-phase and out-of-phase components with the motion by Fourier analysis.

$$Y = Y_{in}\sin(\omega t) + Y_{out}\cos(\omega t) \tag{4}$$

$$K = K_{in}\sin(\omega t) + K_{out}\cos(\omega t)$$

$$N = N_{in}\sin(\omega t) + N_{out}\cos(\omega t)$$

Therefore, hydrodynamic derivatives for pure roll can be expressed as,

$$Y_{\dot{p}} = -\frac{Y_{in}}{\phi_0\omega^2}; \quad Y_p = \frac{Y_{out}}{\phi_0\omega}$$

$$K_{\dot{p}} = -\frac{K_{in}}{\phi_0\omega^2}; \quad K_p = \frac{K_{out}}{\phi_0\omega} \tag{5}$$

$$N_{\dot{p}} = -\frac{N_{in}}{\phi_0\omega^2}; \quad K_p = \frac{N_{out}}{\phi_0\omega}$$

2.4 Numerical simulation

This study uses a commercial CFD program of STAR CCM+. The assumption that the flow was incompressible, the governing equation consists of continuity and momentum, these equations are to simulate the viscous turbulent flow. The motion of a ship is generated following to Eq. (1). The computational domain is created to be sufficiently large to avoid backflow. Therefore, the inlet and outlet boundaries are located 2Lpp upstream and 4Lpp downstream from midship. The sides and bottom boundaries are positioned 2Lpp from the center plane and 1.5Lpp from the water plane. Furthermore, the physical condition are applied for each boundary. The velocity inlet condition is assigned for inlet, and sides boundaries. The outlet boundary specifies the pressure outlet. The symmetry condition is set for side boundaries. The no-slip condition is applied on the wall. In addition, cylindrical covers surrounding the ship as an overset region to carry out the motion. Fig. 4 shows the boundary domain and boundary condition for simulation.

The computational grid is generated by hexahedral dominant meshes. A trimmed cell mesher is used to create the volume grids while a surface remesher is applied to obtain a high-quality surface mesh. The ship's surface is covered with 10 layers of prismatic cells to resolve the surface boundary layer by applying a prism layer mesh motion. The height of first

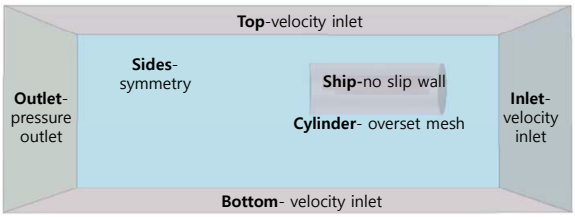

Fig. 4 Boundary domain and condition

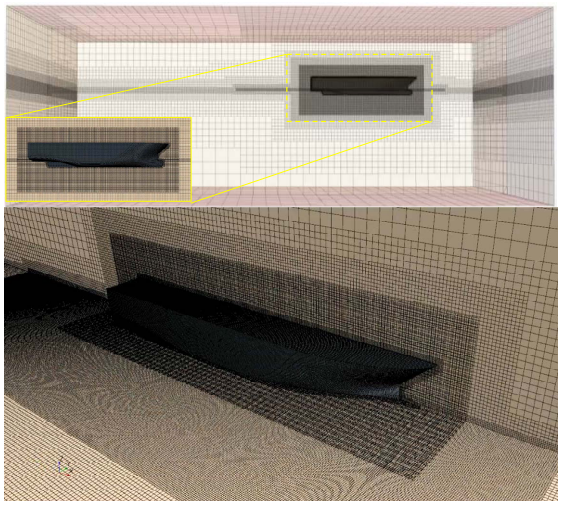

Fig. 5 Mesh generation

element is calculated based on y+ value of boundary layer. Oh and Kang (1992) proposed the y+ value about 3000 ~ 5000 for Reynolds number of 1.0E+09. Using that reference, the height of first element is 8.0 mm corresponding to y+ = 1500 and Reynolds number of 1.5E+08. Fig. 5 presents the mesh generation for the computational domain of the pure roll motion.

The closure of the turbulence model is achieved using the $k-\omega$ SST (Shear Stress Transport) turbulence model because it is good behavior in resolving adverse pressure gradients and separating flow around the ship. The SIMPLE (Semi-implicit method for pressure-linked equation) algorithm is applied to solve the pressure-velocity coupling. VoF (Volume of Fluid) method is adopted to capture the free surface flow around the ship. Time step of 0.005 s was selected according to ITTC recommended (2011) that Reynold stress turbulence models is approximate to (0.001~ 0.0025)L/U.

3. Results and Discussions

3.1 Numerical uncertainty analysis

Before proceeding to methodical computational, it is necessary to perform a verification study. The verification study is executed based on the Grid Convergence Index (GCI) method developed by Roache (1998). The discretization error caused by grid size is evaluated for the pure roll case with p' equal to 0.5. The mesh quantities are given as percentages in terms of a base size in order to refine the grid as systematically as possible. The grid refinement is achieved by applying a refinement factor $r_G = \sqrt{2}$ to the based size. The refinement factor is kept by reducing and increasing cell number on free refinement regions like the free surface, surface ship, and overlap area around the ship. Three grid sets of coarse, medium, and fine grids are used with elements approximately 4.9 million, 6.5 million, and 8.7 million, respectively. The convergence ratio is defined based on the changing solution value between medium-fine ($\varepsilon_{i,21} = \phi_{i,2} - \phi_{i,1}$) and coarse-medium ($\varepsilon_{i,32} = \phi_{i,3} - \phi_{i,2}$) as,

$$R_i = \frac{\varepsilon_{i,21}}{\varepsilon_{i,32}} \tag{6}$$

The order of discretization and the GCI are expressed in Eqs. (7) and (8). Safety factor 1.25 in Eq. (8) is selected by Roache (1998).

$$p = \frac{1}{\ln(r_G)}\left|\ln\left|\frac{\varepsilon_{32}}{\varepsilon_{21}}\right|\right| \tag{7}$$

$$GCI_{ij}^{fine} = \frac{1.25 e_a^{21}}{r^p - 1} \tag{8}$$

p and where, $\varepsilon_{ij} = \phi_i - \phi_j$ and ϕ denote the solution of fine, medium, and coarse input parameters. $e_{ij} = |(\phi_j - \phi_i)/\phi_j|$ is the approximate relative error.

Normally, the verification of the static simulations is focused on constant forces and moments, while the dynamic simulations cover the verification of time series for forces and moments in the time. Therefore, instead of marking the verification on the time series directly, it is recommended to approximate the time series of the forces and moments with derivatives of in-phase and out-of-phase.

The solution of the pure roll simulation with three different grids show a monotonic convergence with the convergence ratio is found 0.673 which indicates the effects of the grid change are accepted to be small between grids system. Table 2 summarizes the results of the grid dependence for the

Table 2 Mesh convergence study for derivatives generated by pure roll

Derivatives	p	GCI_{fine}^{21} (%)
Y_{in}	2.77	2.08
Y_{out}	1.68	3.63
K_{in}	0.62	1.27
K_{out}	1.64	1.78
N_{in}	1.99	3.24
N_{out}	2.43	2.75

in-phase and out-of-phase of derivatives generated by the

pure roll. The numerical uncertainties in the fine-grid solution GCI of derivatives are less than 5% and order of discretization is less than 3. According to ITTC recommended (2017), the accuracy of order of discretization equal to 2 with factor of safety of 1.25 is applied. This indicated that the approximate relative errors among grid density sets are small. Thus a medium grid density is chosen for simulation, which contains about 6.5 million elements.

3.2 Pure roll result

Fig. 6 shows the time histories of sway force (Y), roll moment (K), and yaw moment (N) generated by the pure roll at different dimensionless roll angular velocities at constant speed of 13 knots. In which, the dimensionless of force, moments is calculated by $Y' = F/(0.5\rho U^2 L^2)$ and $K', N' = K, N/(0.5\rho U^2 L^3)$, respectively. Three periods when the time is stable are captured for each force and moment. The results indicates that the amplitude of hydrodynamic forces and moments increase as the roll angular velocity is increased. The frequency of the motion is kept constant during all cases and is equal to 3.125 rad/s. The fitting forces and moments of the pure roll are implemented by distinguishing the in-phase and out-of-phase as shown in Eq. (1). In-phase component which refers to the amplitudes taken in-phase with roll angle (ϕ) determines the force and moment due to angular acceleration ($\dot{p}$) while out-of-phase component which indicates to the amplitude taken 90° phase shifted with roll angle (ϕ) determines the force and moment due to angular velocity (p). In which, the in-phase component is used to obtain the added mass derivatives and the out-of-phase component is used to take the damping derivatives.

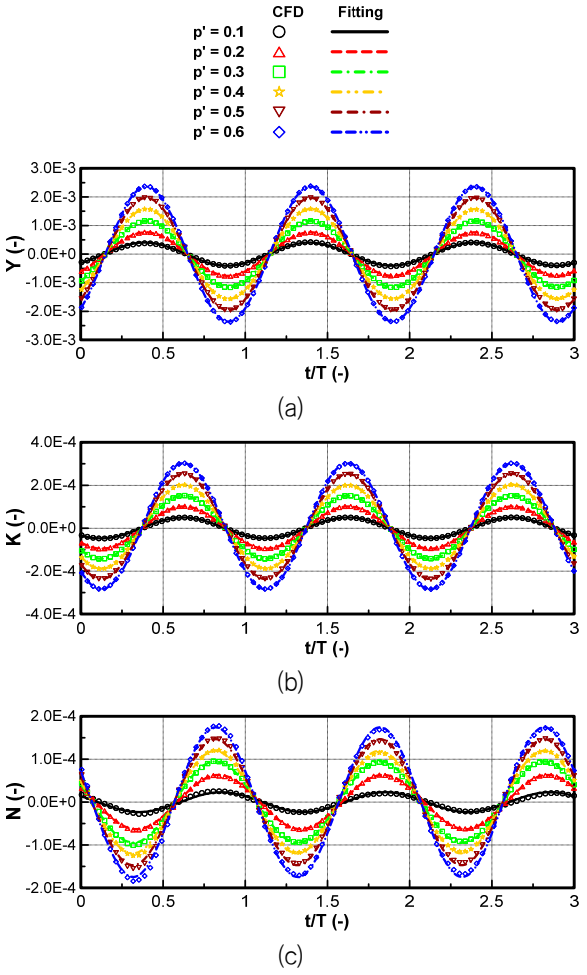

Fig. 6 Time histories of hydrodynamic forces and moments during pure roll

Fig. 7 presents the in-phase amplitudes of pure roll with respect to dimensionless roll angular acceleration calculated by $\dot{p}' = (p'\omega L)/U$. It can be seen that the in-phase results give linear reactions. The added mass derivatives of sway, roll, and yaw relative to the roll angular acceleration are then taken.

Fig. 8 shows the out-of-phase amplitudes of the pure roll with respect to dimensionless roll angular velocity. The out-of-phase results also give a nearly linear reaction. Therefore, the non-linear terms of Y_{ppp}, K_{ppp}, and N_{ppp} are very small. The damping derivatives of sway, roll, and yaw relative to the roll angular velocity are obtained.

Fig. 9 shows the volume fraction of the middle section

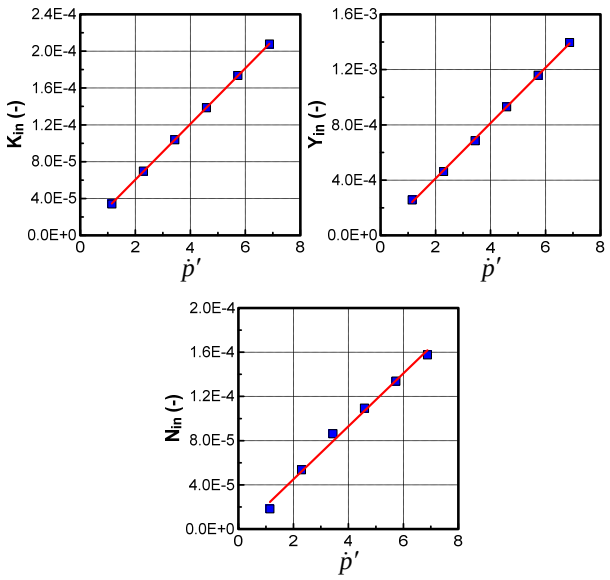

Fig. 7 In-phase results of pure roll

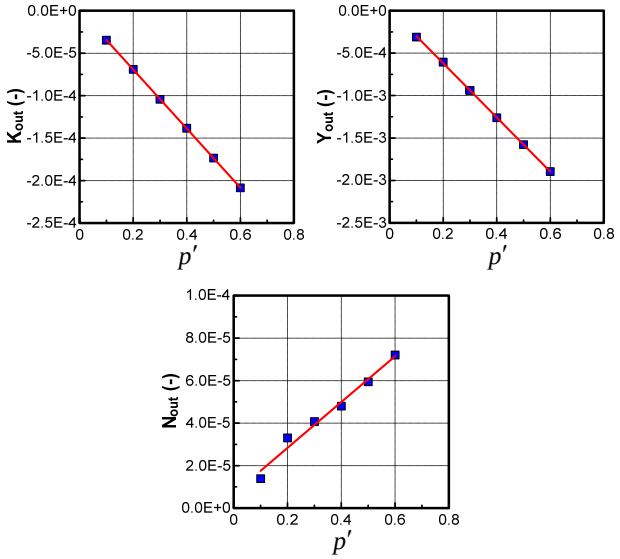

Fig. 8 Out-of-phase results of pure roll

Table 3 Hydrodynamic derivatives generated by pure roll

HD Derivatives	Value
$Y_{\dot{p}}$	-2.76E-03
$K_{\dot{p}}$	-4.06E-04
$N_{\dot{p}}$	-3.02E-04
Y_p	-1.14E-02
K_p	-1.27E-03
N_p	4.48E-04
Y_{ppp}	-3.40E-05
K_{ppp}	-8.23E-06
N_{ppp}	-2.39E-04

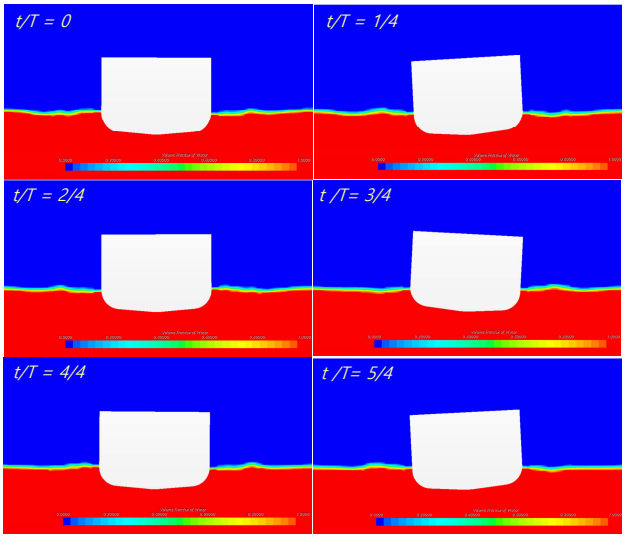

Fig. 9 Volume fraction during pure roll

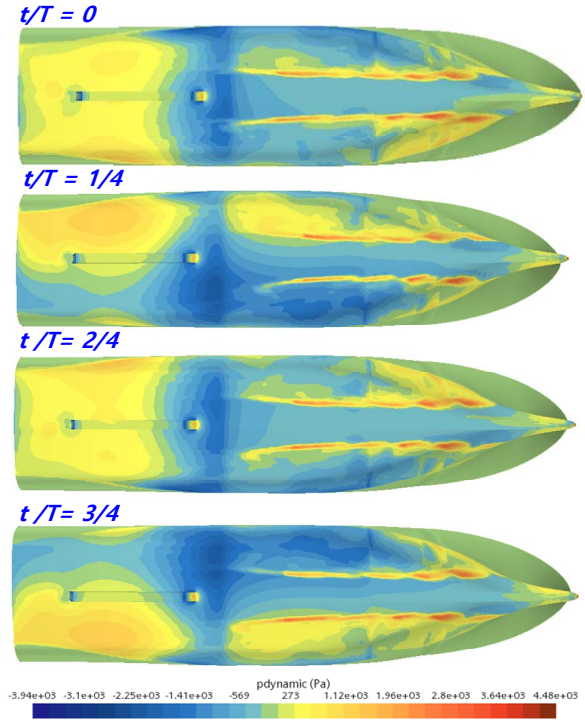

Fig. 10 Dynamic pressure distribution

during pure roll at different times. It describes the ship's motion throughout one period. Fig. 10 presents the dynamic pressure distribution when the ship is reaching the peak (t/T = 1/4 and t/T = 3/4) and lowest (t/T = 2/4) during the pure roll motion. It is defined as equation of $P_d = \frac{\rho v^2}{2}$. Dynamic pressure contours suffer an obvious deformation as the ship is converted from the starboard and port sides.

4. Conclusion

This study presented the pure roll test to predict the added mass and damping derivatives relative to the roll component using CFD simulation in STAR CCM+. An autonomous surface ship designed to carry the containers with small draft and high speed was used. Because the specification of the ship indicated a feature that is much affected by roll moment. The pure roll motion in CFD method was verified by the mesh independence study. The approximate relative errors of in-phase and out-of-phase derivatives was small among grid density sets. Therefore, the pure roll test at different dimensionless angular velocity was simulated with the medium grid density. The results showed that the amplitude of forces and moments increase as the roll angular velocity is increased. Then, the added mass and damping derivatives relatives to roll moment were taken by distinguishing the

in-phase and out-of-phase components. These derivatives will be used to complemented the roll moment in the 4-DOF motion equations.

Acknowledgements

This research was supported by the 'Development of Autonomous Ship Technology(PJT201313,Development of Autonomous Navigation System with Intelligent Route Planning Function)' funded by the Ministry of Oceans and Fisheries (MOF, Korea).

References

Fukui, Y., Yokota, H., Yano, H., Kondo, M., Nakano, T. and Yoshimura, Y., 2016. 4-DOF mathematical model for manoeuvring simulation including roll motion. *Journal of the Japan Society of Naval Architects and Ocean Engineers,* 24(0), pp.167-179.

ITTC., 2011. ITTC-Recommended procedures and guidelines. *Practical Guidelines for Ship CFD Application*.

ITTC., 2017. ITTC-Recommended procedures and guidelines. *Uncertainty Analysis in CFD Verification and Validation Methodology and Procedures*.

Kim, D.H., Baek, H.M., Lee, S.K. and Kim, E.S., 2021. Development of apparatus for pure roll-motion test of underwater vehicles. Journal of Navigation and Port Research, 45(1), pp.16-25.

Oh, K.J. and Kang, S.H., 1992. Full scale Reynolds, Number effects for the viscous flow around the ship stern. *Journal of Computational Mechanics*, 9(2). pp.85-94.

Park, J.Y., Kim, N., Rhee, K.-P., Yoon, H.K., Kim, C., Jung, C., Ahn, K. and Lee, S., 2015. Study on coning motion test for submerged body. *Journal of Ocean Engineering and Technology*, 29(6), pp.436-444.

Roache, P.J., 1998. *Verification and validation in computational science and engineering.* Albuquerque, NM: Hermosa.

Son, K. and Nomoto, K., 1981. On the coupled motion of steering and rolling of a high speed container ship. *Journal of the Society of Naval Architects of Japan*, 1981(150), pp.232-244

Yasukawa, H. and Yoshimura, Y., 2014. Roll-coupling effect on ship maneuverability. *Hip Technology Research*, 61(1), pp.16-32.

Yasukawa, H., Sakuno, R. and Yoshimura, Y., 2019. Practical maneuvering simulation method of ships considering the roll-coupling effect. *Journal of Marine Science and Technology(Japan)*, 24(4), pp.1280-1296.

Yoshimura, Y., 2011. Effect of roll motion on ship manoeuvrability by a rudder to yaw response equation. *Journal of the Japan Society of Naval Architects and Ocean Engineers*, 13, pp.11-18.


Thi Loan Mai


Anh Khoa Vo


윤 현 규